FABRICATION AND CHARACTERIZATION OF PASSIVATED PEROVSKITE SOLAR CELL WITH ZINC OXIDE QUANTUM DOTS AS ELECTRON TRANSPORT LAYER

AHLAAM TAHER NOMAAN SAEED MOHAMMED

UNIVERSITI SAINS MALAYSIA

2025

FABRICATION AND CHARACTERIZATION OF PASSIVATED PEROVSKITE SOLAR CELL WITH ZINC OXIDE QUANTUM DOTS AS ELECTRON TRANSPORT LAYER

by

AHLAAM TAHER NOMAAN SAEED MOHAMMED

Thesis submitted in fulfilment of the requirements.
for the degree of
Doctor of Philosophy

February 2025

ACKNOWLEDGEMENT

In The Name Of All, Most Gracious, Most Merciful

All praise is for almighty Allah who gave me strength, patience, and inspiration to complete this thesis. Without his Mercy this thesis would not have come into existence.

I would like to express my sincere gratitude to my supervisor, Dr. Mohd Marzaini Mohd Rashid for his creative guidance, intellectual support, patience, and insightful feedback that have been instrumental in shaping this thesis. I am particularly grateful for his wonderful attitude, willingness to answer any questions and encouragement during my doctoral study.

My heartfelt gratitude also goes to my wonderful family - my parents for their continuous prayers and support, my husband Dr. Anas for standing by me and helping me step by step, and my sons, brothers, and sisters for their encouragement and support. Their unwavering love and belief in me fueled my perseverance and helped me overcome obstacles.

I would like to express my great appreciation and acknowledgement to all Nano optoelectronic research laboratory (NOR Lab) staff for their technical support during experiments and characterizations.

To all my amazing friends, thank you for being my support system throughout this journey. Your friendship provided me with much-needed laughter, encouragement, and a sense of community. I am especially grateful to Shawbo, Sameen, Syahida and Nurizati for all your support during this journey.

Ahlaam Taher

USM, Malaysia 2024

TABLE OF CONTENTS

ACKNOWLEDGEMENT ii

TABLE OF CONTENTS iii

LIST OF TABLES viii

LIST OF FIGURES ix

LIST OF SYMBOLS xviii

LIST OF ABBREVIATIONS xix

LIST OF APPENDICES xxi

ABSTRAK xxii

ABSTRACT xxiv

CHAPTER 1 INTRODUCTION 1

1.1 Introduction 1

1.2 Perovskite Solar Cells 1

1.3 Problem Statement 3

1.4 Research Focus 4

1.5 Research Objectives 5

1.6 Originality of the Study 5

1.7 Thesis Outline 6

CHAPTER 2 THEORETICAL BACKGROUND AND LITERATURE REVIEW 8

2.1 Introduction 8

2.2 Solar Cell Generations 8

2.3 Classification of Perovskite Solar Cells According to Their Architecture 10

2.4 The Carrier Transport Materials 13

2.4.1 The Hole Transport Layer 13

2.4.2 Electron Transport Layer 14
2.4.3 Electrodes 14
2.5 Performance Properties and Main Parameters in PSCs 15
2.5.1 Open-Circuit Voltage 16
2.5.2 The Short-Circuit Current 16
2.5.3 Fill Factor 17
2.5.4 The Power Conversion Efficiency 18
2.5.5 Series Resistance and Shunt Resistance 18
2.6 Working Principle of PSCs 19
2.7 Properties of Perovskite as Photo-Absorber Layer 21
2.8 Type and Role of the HTLs in PSCs 22
2.9 Type and Role of the ETL in PSCs 23
2.10 Properties of ZnO as ETL in PSCs 24
2.11 Strategies for Enhancing ZnO ETLs 31
2.11.1 Doping 32
2.11.2 Bilayer Structures 35
2.11.3 Interface Modification 37
2.11.4 Morphology Management 46
CHAPTER 3 METHODOLOGY AND CHARACTERIZATION INSTRUMENTS 52
3.1 Introduction 52
3.2 Materials 54
3.2.1 Chemicals Used to Prepare Solution-Based ZnO QDs 54
3.2.2 Chemicals Used to Prepare Lead Halide Perovskite Films 55
3.2.3 Materials Used for Interface Passivation 55
3.2.4 Chemicals Used to Prepare Hole Transport Layer 56
3.3 Synthesis of Solution-Based ZnO Quantum Dots 57
3.4 Substrate Cutting, Etching, and Cleaning 59

3.5 Preparation of ZnO QD-based Thin Films 60

3.6 Preparation of Lead Halide Perovskite Films 62

3.7 Fabrication Process of n-i-p Perovskite Solar Cells 63

3.7.1 Substrate Etching and Preparation of ZnO QD-based Film as ETL 64

3.7.2 Preparation of Passivation Layer on ZnO QD-based Film 64

3.7.2(a) Polyethyleneimine as Passivation Layer 65

3.7.2(b) Aluminum Oxide as Passivation Layer 65

3.7.3 Preparation of Perovskite Film as Photoactive Layer 66

3.7.4 Preparation of Spiro-OMeTAD as HTL 67

3.7.5 Deposition of Silver Metal as Back Electrode 68

3.8 Characterization Instruments 70

3.8.1 Transmission Electron Microscope 71

3.8.2 Field Emission Scanning Electron Microscope 72

3.8.3 Atomic Force Microscope 73

3.8.4 X-ray Diffraction 74

3.8.5 Ultraviolet-Visible Spectrophotometer 76

3.8.6 Photoluminescence Spectrophotometer 79

3.8.7 X-ray Photoelectron Spectroscopy 80

3.8.8 Fourier Transform Infrared Spectroscopy 82

3.8.9 Photoelectric Measurement System 83

3.8.10 Solar Simulator System 86

CHAPTER 4 RESULTS AND DISCUSSIONS: SYNTHESIS OF ZnO QUANTUM DOT-BASED THIN FILM AS ELECTRON TRANSPORT LAYER ……..... 88

4.1 Introduction 88

4.2 Solution-based ZnO QDs 88

4.3 ZnO QD-based Thin Films Prepared at Different Thicknesses 91

4.3.1 Surface Morphology Analysis 92

4.3.2 Structural Analysis 96

4.3.3 UV-Vis Analysis 98

4.4 Influence of Annealing Temperature on Quantum Dot Nature of ZnO Thin Films 101

4.4.1 Surface Morphology Analysis 101

4.4.2 Structural Analysis 106

4.4.3 UV-Vis Analysis 109

4.4.4 Photoluminescence Analysis 111

4.5 Influence of Surface-to-Volume Ratio of Quantum Dots on Photoelectric Properties of ZnO Thin Films 119

4.5.1 Current-Voltage Characteristics 119

4.5.2 Photoelectric Parameters 121

4.6 Summary 127

CHAPTER 5 RESULTS AND DISCUSSIONS: GROWTH OF PEROVSKITE FILMS AND FABRICATION OF PEROVSKITE SOLAR CELLS 128

5.1 Introduction 128

5.2 Growth of Perovskite Films at Different Temperatures 128

5.2.1 Surface Morphology and Elemental Analysis 128

5.2.2 Structural Analysis 131

5.2.3 Optical Properties Analysis 132

5.3 Influence of Anti-Solvent on Growth of Perovskite Films 134

5.3.1 Surface Morphology and Elemental Analysis 135

5.3.2 Structural Analysis 141

5.3.3 UV-Vis Analysis 142

5.4 Growth of Perovskite Film Over ZnO QD-Based Film for Photovoltaic Application 143

5.4.1 Surface Morphology and Structural Analysis 144

5.4.2 Optical Properties Analysis 146

5.4.3 XPS Analysis 148

5.4.4 Photovoltaic Characteristics of Perovskite Solar Cells 152

5.5 Improved Photovoltaic Performance by Enhancing Perovskite Surface Morphology 158

5.5.1 Enhancing Perovskite Film Growth Over ZnO QD-ETL 159

5.5.1(a) Surface Morphology Analysis 159

5.5.1(b) Structural Analysis 161

5.5.1(c) Optical Analysis 162

5.5.2 Fabrication of PSC based on Enhanced Perovskite Film: Effect of Interface Passivation 163

5.5.2(a) Surface Morphology 164

5.5.2(b) Structural Analysis 166

5.5.2(c) UV-Vis Analysis 167

5.5.3 Photovoltaic Performance of Enhanced Perovskite Solar Cells 168

5.5.4 Influence of Light Intensity on Photovoltaic Performance 177

5.6 Summary 180

CHAPTER 6 CONCLUSIONS AND FUTURE RECOMMENDATIONS 182

6.1 Conclusions 182

6.2 Recommendations for Future Research 184

REFERENCES 186

APPENDICES

LIST OF PUBLICATIONS

LIST OF TABLES

Page

Table 2.1 Summary of the ZnO ETL in devices layout 26

Table 4.1 Lattice constants and crystallite size of ZnO QD-based thin films prepared at various thicknesses. 98

Table 4.2 Optical parameters extracted from UV-Vis analysis 100

Table 4.3 Structural properties of As-coated ZnO film and ZnO films annealed at different temperatures. 108

Table 5.1 Elemental composition of Pb, I and C in the $MAPbI_3$ films prepared at different temperatures. 131

Table 5.2 Elemental composition of Pb, I and C in the $MAPbI_3$ films prepared at different temperatures. 138

Table 5.3 Photovoltaic characteristics of non-passivated and interface passivated HTL-free and HTL-included devices. 154

Table 5.4 Photovoltaic parameters of the optimized PSC (D4). 158

Table 5.5 Photovoltaic parameters of non-passivated and interface passivated perovskite solar cells. 170

Table 5.6 Overall comparison of the photovoltaic performance of the fabricated PSCs. 175

Table 5.7 Photovoltaic parameters of ITO/ZnO QD/1wt% PEI/ $CH_3NH_3PbI_3$-M/Spiro-OMeTAD/Ag devices measured within four weeks. 176

LIST OF FIGURES

Page

Figure 1.1 Crystal structure of organic-inorganic halide perovskite [18]. 2

Figure 1.2 Schematic illustration of the research focus of this thesis. 4

Figure 2.1 The three generations of solar cells.....9

Figure 2.2 Different architectures of Perovskite solar cells with and without hole transport layer [45, 46] 12

Figure 2.3 I-V characteristic response of perovskite solar cell showing the basic parameters of the solar device [65].....16

Figure 2.4 Energy band diagram of a typical n-i-p perovskite solar cell [72].....20

Figure 2.5 Energy level diagrams of HTL and ETL materials used in PSCs [84].....23

Figure 2.6 (a) PSCs device structure, (b) Cross-section of PSC based on the ZnO nanorod electrode, and (c) J-V curve [113].....29

Figure 2.7 Illustrates the structure of PSC. The provided images show a cross-sectional TEM image of a PSC made of P1 and c-ZnO. The c-ZnO layer has a thickness of around 30 nm. Additionally, high-resolution cross-sectional TEM images of a PSC based on P1 and c-ZnO are displayed, along with J-V curves of devices using different ZnO ETLs based on P1, P2, and P3. [115].....30

Figure 2.8 Various methods for optimization procedures of PSCs, which include dopant and additive inclusion, interface structuring, and bilayer engineering.....31

Figure 2.9 The provided photos include SEM views of (a) undoped ZnO, (b) enlarged undoped ZnO nanofibers, (c) Mg-ZnO nanofibers, (d) magnified Mg-ZnO nanofibers, (e) a photovoltaic device based on Mg-ZnO nanofibers, (f) The nano-fibers are made of Mg-ZnO with a 5% Mg-doping , (g) The band gap spectra of ZnO, 1% Mg-ZnO,

2% Mg-ZnO, and 3% Mg-ZnO are being analysed and (h) The J-V curve is shown for undoped and 1%, 2%, and 3% Mg-ZnO PSCs [125]. 34

Figure 2.10 (a) Device structure of PSCs, (b) Energy band diagram, (c) Top view of Perovskite layer using SEM image, and (d) J-V curves of the planar PSC [126]. 36

Figure 2.11 MAPbI 3 solar cell with the Al_2O_3 passivation layer. (a) An SEM cross-sectional image of the perovskite solar cell comprising FTO/c-TiO_2 / A- Al_2O_3/mp-TiO_2 /$MAPbI_3$ /PTAA/Au. (b) A schematic depicting heterojunction in the mp-TiO_2 based perovskite solar cells. (c) J–V curves. (d) PL emission spectra of the $MAPbI_3$ films (without PTAA) with different substrates. Reduced recombination is observed with mp-TiO_2 and A-Al_2O_3/mp-TiO_2 substrates [139]. 39

Figure 2.12 Device structure with morphology, (a) Schematic diagram of the designed PSC, (b) Cross-sectional FESEM image of PSC, (c) Top view SEM image of ZnO, (d) HRTEM image. 40

Figure 2.13 (a) J–V curves of ALD- Al_2O_3, (b) log plots of the I–V curves of ZnO ETM, (c) Schematic diagram of the ALD- Al_2O_3 coating on the ZnO NRs, (d) EQE spectra of the best device fabricated without the ALD cycle and that with two ALD cycles, (e) J–V curves of the PSCs fabricated using the as-grown ZnO NRs with length of 910 nm, the annealed ZnO NRs, and the annealed ZnO NRs with ALD- Al_2O_3 coating, (f) Histogram showing the reproducibility of the annealed ZnO NRs-based PSCs fabricated with two ALD cycles and without the ALD cycles [106]. 41

Figure 2.14 XRD of perovskite film PEI, (a) $PC_{61}BM$-coated ZnO, (b) PEI-coated ZnO (c) intensity ratio of perovskite on ZnO/PEI-perovskite on ZnO/$PC_{61}BM$, and (d) schematics of the growth of perovskite deposited on $PC_{61}BM$-coated ZnO and PEI-coated ZnO during thermal annealing [110]. 43

Figure 2.15 SEM images and grain size distribution of perovskite film deposited on (a) $PC_{61}BM$-coated ZnO, (b) PEI coated ZnO, (c) SEM images of perovskite film deposited on $PC_{61}BM$-coated ZnO with thermal annealing at 100 °C, and (d) with thermal annealing at 100 °C for 1 h [110]. 44

Figure 2.16 (a) Schematic diagram of the device structure, (b) Energy level diagram showing the energy level concerning vacuum level for the different components of the PSC, (c) SEM image, and (d) J-V curve of PSC device [147]. 45

Figure 2.17 ZnO NPs with different morphologies seen in SEM images: (a) and (b) tetrapod structures, (c) variable diameter structures, (d) nanosheets, (e) nanoshells, (f) multipods, (g)–(i) nanorods [156]. 48

Figure 2.18 FESEM of perovskite layer that was formed on three different types of films: (a) virgin mp-TiO_2, (b) ZQDs modified mp-TiO_2, and (c) TQDs modified mp-TiO_2. The photos are labelled as (d–f). The provided photos show cross-sectional SEM images of a fully assembled device composed of PT, PZT, and PTT structures. Additionally, the graph labelled (g) J-V curves of the PSCs, and The relationship between the output current density at the maximum power point and time, as well as (h) the integrated current data and IPCE of the related devices [163].....50

Figure 2.19 (a) ITO-PET/Gr device, (b)Fabricated ITO-PET/Gr/ZnO-QDs(APjet)/CH3NH3PbI3/spiro-MeOTAD/Ag flexible, (c) J−V curves, and (d) IPCE [111].....51

Figure 3.1 Flowchart illustrating the experimental procedure for fabrication of perovskite solar cells.....53

Figure 3.2 Chemicals used to prepare solution-based ZnO QDs. (a) Zinc acetate dihydrate (d) Potassium hydroxide pellets (e) Methanol. 54

Figure 3.3 (a)Methylammonium iodide (b) lead acetate trihydrate (c) Anhydrous N, N-dimethylformamide (DMF) (d) Dimethyl sulfoxide (DMSO).....55

Figure 3.4 Materials used for interface passivation. (a) Aluminum oxide target (b) Polyethyleneimine. 56

Figure 3.5 Precursors used for preparation hole transport layer. (a) (Spiro-OMeTAD), (b) 4-tert-butylpyridine (TBP) additive, (c) Bis(trifluoromethane)-sulfonimide lithium salt (Li-TFSI). 57

Figure 3.6 Schematic illustration of preparation solution-based ZnO QDs using solvothermal route. 58

Figure 3.7 A mixture of zinc acetate and potassium hydroxide solution at 60 ^{o}C (a) in the beginning of reaction (b) and after 2.5 h. (c) Obtained ZnO QDs solution. 58

Figure 3.8 preparation and cleaning ITO substrate. (a) Glass cutter (b) Etching ITO substrate (c) cleaning ITO etched substrates in acetone, ethanol, and DI water. 59

Figure 3.9 plasma cleaning unit (PLASMAPREP 100) 60

Figure 3.10 Spin coater machine (CHEMAT TECHNOLOGY, KW-4A) used to prepare ZnO QD-based films. 61

Figure 3.11 MBRAUN UNIlab glovebox inside which perovskite films were prepared. 62

Figure 3.12 (a) A digital photograph of perovskite solution (b) As-coated perovskite film (c-e) Perovskite films prepared at different temperatures: (c) 60 ^{o}C (d) 100 ^{o}C (e) 140 ^{o}C. 63

Figure 3.13 Etching ITO substrate and preparation of ZnO QD-based film as ETL. 64

Figure 3.14 Preparation of PEI passivation layer on ZnO QD-based ETL. 65

Figure 3.15 RF sputtering system (Model: Auto HHV 500) used to deposit Al_2O_3 passivation layer on ZnO QD-based film. 66

Figure 3.16 Preparation of perovskite film as a photoactive layer on a passivated ZnO QD-based ETL. 67

Figure 3.17 Preparation Spiro-OMeTAD layer over perovskite film as HTL. 68

Figure 3.18 Edwards 306 evaporation system used to deposit Ag electrode. 69

Figure 3.19 Digital photographs of the fabricated perovskite solar cell (a) and (b). (c) Schematic illustration of the overall architecture of the PSC.....70

Figure 3.20 (a) A digital photograph of TEM system (Carl Zeiss Libra 120) (b) Schematic illustration of its working principle [164]. 71

Figure 3.21 A digital photo of FESEM system (Model: FEI Nova NanoSEM 450) (b) Schematic demonstration of the operating principle [165]. 73

Figure 3.22 (a) A photograph of AFM (b) Schematic illustrating working principle of AFM [166]. 74

Figure 3.23 (a) A digital photo of XRD system (PANalytical X'pert PRO MRD PW3040/60) (b) Bragg's condition (c) X-ray diffraction from a crystallite [172]. 76

Figure 3.24 (a) A digital photograph of UV-Vis spectrophotometer (b) Working principle illustration of the UV-Vis system [177]. 78

Figure 3.25 (a) Jobin Yvon HR 800 UV photoluminescence (PL) system (b) A proprietary PL system belongs to Dr. W. Maryam's group. 80

Figure 3.26 (a) A digital photo of Kratos Axis Ultra-DLD XPS system (b) Schematic diagram illustrating working principle of XPS instrument [178]. 81

Figure 3.27 (a) photograph of Perkin Elmer Frontier ATR-FTIR spectrophotometer and (b) its working principle [179].....83

Figure 3.28 (a) Digital photographs and (b) FESEM image of metal masks used to evaluate photoelectric properties of ZnO QD-based films (c) A digital photo of the photodetection measurement system (d) Schematic illustrating the photodetection setup of the fabricated perovskite solar cell.....85

Figure 3.29 Solar simulator measurement system (Forter Transient Measurement System) for evaluating power conversion efficiency of the fabricated PSCs. 87

Figure 4.1 (a) XRD pattern of powder-based ZnO QDs. (b) TEM image of powder-based ZnO QDs. (c) TEM image of solution-based ZnO QDs. (d) and (e) Absorbance and Tauc's plot of powder-based and solution-based ZnO QDs, respectively. 90

Figure 4.2 Cross-sectional FESEM images of ZnO QD-based thin films coated over ITO substrate at various thicknesses. 91

Figure 4.3 Low magnification and high magnification FESEM images of ZnO QD-based thin films coated at (a) 20 nm, (b) 60 nm, (c) 90 nm. 94

Figure 4.4 2D and 3D AFM images of (a) ITO bare and ZnO QD-based thin films coated at thickness of (b) 20 nm, (c) 60 nm, (d) 90 nm. 95

Figure 4.5 Grain size and RMS surface roughness versus film thickness.....96

Figure 4.6 XRD patterns of ITO substrate and ZnO QD-based films coated over ITO substrate at various thicknesses. 97

Figure 4.7 UV-Vis analysis of ITO substrate and ITO/ZnO QD-based films coated at various thicknesses. (a) Absorbance spectra. (b) Tauc' plot. (c) Transmittance spectra. (d) Reflectance spectra. 100

Figure 4.8 FESEM micrographs along with particle size distribution of the as-coated ZnO and ZnO films annealed at different temperatures. 103

Figure 4.9 2D and 3D AFM images of as-coated ZnO film (a) and ZnO films annealed at 250 ^{o}C (b), 350 ^{o}C (c), and 450 ^{o}C (d). 105

Figure 4.10 Average grain size and RMS surface roughness dependency on annealing temperature. 106

Figure 4.11 XRD patterns of the as-coated ZnO film and ZnO films annealed at different temperatures. 107

Figure 4.12 (a) Transmittance (b) Reflectance spectra of the as-coated ZnO film and ZnO films annealed at different temperatures (c) Tauc's plot of the as-coated film and films annealed at different temperatures. 110

Figure 4.13 (a) PL spectra of all ZnO thin films (b – e) PL spectra of as-coated ZnO film and ZnO films annealed at 250, 350 and 450 ^{o}C, respectively. 113

Figure 4.14 The intensity ratio of yellow to green emission at different annealing temperatures..... 116

Figure 4.15 Schematic diagram of (a) two adjacent ZnO nanograin having small size (b) two adjacent ZnO nanograin with larger size (c) transitions related to oxygen vacancies in the bulk and at the grain-boundary depleted region. 118

Figure 4.16 (a) I-V characteristics of ZnO MSM PDs in the dark and under illumination with wavelength of 365 nm (b) The enlarged I-V characteristics of the as-coated PD and the PD annealed at 250 ^{o}C in the dark and under UV light illumination. 120

Figure 4.17 Transient photocurrent of the as-coated PD and the PDs annealed at different temperatures (a-d). (e) the PDCR and responsivity as a function of annealing temperature. 122

Figure 4.18 Rising edge (a) and falling edge (b) of the transient photocurrent of the as-coated PD and annealed PDs. (c) the rise time and fall time at different temperatures. 124

Figure 5.1 (a) FESEM and AFM images of $MAPbI_3$ perovskite thin films prepared at different temperatures. (b) EDX mapping analysis of the $MAPbI_3$ thin film annealed at 100 ^{o}C..... 130

Figure 5.2 XRD patterns of PbI_2 and $MAPbI_3$ perovskite thin films prepared at different temperatures. 132

Figure 5.3 UV-Vis spectra (a), ASF plots (b), and PL spectra (c) of $MAPbI_3$ perovskite thin films prepared at different temperatures. 134

Figure 5.4 FESEM images of perovskite films treated with different anti-solvents. (a) chlorobenzene (b) chloroform (c) toluene (d) iso-propanol alcohol. 137

Figure 5.5 Digital photographs of $MAPbI_3$ perovskite films treated with different anti-solvents..... 138

Figure 5.6 2DAFM images of anti-solvent-treated $MAPbI_3$ perovskite films. .140

Figure 5.7 XRD patterns of $MAPbI_3$ perovskite films treated with different anti-solvents. 142

Figure 5.8 UV-Vis absorbance spectra of $MAPbI_3$ perovskite films treated with different anti-solvents. 143

Figure 5.9 FESEM images of perovskite film (i), ZnO/perovskite film (ii), and ZnO/Al_2O_3/perovskite film (iii). (b) XRD patterns of pure perovskite and perovskite coated on non-passivated and passivated ZnO QD-based film. (c) FTIR spectra of non-passivated and passivated ZnO QD-based film. 145

Figure 5.10 (a) UV-Vis absorbance spectra and (b) PL spectra of perovskite, ZnO/perovskite, and ZnO/Al_2O_3/perovskite films. 147

Figure 5.11 XPS spectra of ZnO and ZnO/Al_2O_3 films: (a) Zn 2*p*, (b) Al 2*p*, (c) valence band, and (d) O 1*s*. 149

Figure 5.12 XPS spectra of $CH_3NH_3PbI_3$ prepared on a ZnO/Al_2O_3 film: (a) C 1*s*, (b) N 1*s*, (c) Pb 4*f*, (d) I 3*d*, and (e) valence band. 151

Figure 5.13 (a) J-V characteristics of the fabricated PSCs (b) Power conversion efficiency of non-passivated interface, interface passivated device 153

Figure 5.14 Band alignment of perovskite solar cell architecture (a) without and with (b) ZnO/perovskite interface passivation. 156

Figure 5.15 (a) J-V characteristics under different light intensity (b) and FESEM cross-sectional image of the optimized PSC (D4) (c) schematic diagram of the cross section in Figure (b). 157

Figure 5.16 FESEM images of perovskite film coated over ZnO QD-based ETL without DMSO (a) and with adding different amounts of DMSO (b-f). 160

Figure 5.17 XRD patterns of perovskite film prepared on ZnO QD-ETL at different DMSO/DMF volume ratios. 162

Figure 5.18 UV-Vis absorbance spectra of perovskite film prepared on ZnO QD-ETL at different DMSO/DMF volume ratios. 163

Figure 5.19 FESEM micrographs of $MAPbI_3$ perovskite grown on (a) non-passivated ZnO QD-ETL (b) Al_2O_3 passivated ZnO QD-ETL (c) 1wt% PEI passivated ZnO QD-ETL (d) 2wt.% PEI passivated ZnO QD-ETL (e) 1wt.% PEI passivated ZnO QD-ETL grown over RF-ZnO seed layer. 165

Figure 5.20 XRD patterns of non-passivated and ZnO/$MAPbI_3$ interface passivated with inorganic (Al_2O_3) and organic (PEI) materials.....166

Figure 5.21 UV-Vis absorbance spectra of non-passivated and ZnO/$MAPbI_3$ interface passivated with inorganic (Al_2O_3) and organic (PEI) materials. 167

Figure 5.22 A comparison of (a) J-V and (b) power-V characteristics of non-passivated and interface passivated perovskite solar cells. 169

Figure 5.23 (a) Evolution in the power conversion efficiency of the fabricated PSCs (D1-D9). (b, c) Cross-sectional images of PSCs prepared using DMF solvent (D4) and DMSO added to DMF solvent (D7), respectively. 174

Figure 5.24 I-V characteristic of ITO/ZnO QD/1wt% PEI/ $CH_3NH_3PbI_3$-M/Spiro-OMeTAD/Ag devices measured within four 4 weeks. 176

Figure 5.25 J-V characteristics (a-e) and power conversion efficiency (f) of PSCs versus light intensity. 178

Figure 5.26 P-V characteristics of PSCs versus light intensity. 179

Figure 6.1 (a) Ag contact on top the whole device (b) Ag contact on top the perovskite film 185

LIST OF SYMBOLS

E_g	Energy band gap
V_{OC}	Open circuit voltage
I_{SC}	Short circuit current
FF	Fill factor
P_{max}	Maximum power point
R_{sh}	Series resistance
R_s	Shunt resistance
V_{max}	Maximum voltage
I_{max}	Maximum current
P_{in}	Input power
P_{out}	Output power
η	Efficiency
Å	Angstrom
R%	Reflectance
T%	Transmittance
A	Absorbance
eV	Electron volt
λ	Wavelength
Ω	Ohm
$^{\circ}$C	Degree Celsius
W	Watt
mA	Milliampere
θ	Diffraction angle

LIST OF ABBREVIATIONS

%RH	Relative Humidity
AFM	Atomic force microscopy
Ag	Silver
Al	Aluminium
Al2O3	Aluminium oxide
Ar	Argon
Au	Gold
C.B	Chlorobenzene
C.F	Chloroform
CB	Conduction Band
CCM	Cubic centimeter
CdS	Cadmium sulfide
CuI	Copper(I) iodide
CuO	Copper (II) oxide
CuSCN	Copper(I) thiocyanate
DMF	Dimethylformamide
DMSO	Dimethyl sulfoxide
ETL	Electron transport layer
FAI	Formamidinium Iodide
FESEM	Field emission scanning electron microscopy
FTIR	Fourier Transform Infrared Spectroscopy
FTO	Fluorine tin oxide
HOMO	Highest Occupied Molecular Orbital
HTL	Hole transport layer
IGZO	(Indium–gallium–zinc oxide)
IPA	Iso Propanol
ITO	Indium tin oxide
J-V	Current density–voltage
Li-TFSI	Bis(trifluoromethane)sulfonimide lithium salt
LUMO	Lowest unoccupied Molecular Orbital
MAI	Methylammonium iodide

NiO	Nickel oxide
NPs	NPs Nanoparticles
P3HT	(Poly (3-hexylthiophene 2,5-diyl))
PCBM	(6,6-phenyl-C61-butyric acid methyl ester)
PCE	Power conversion efficiency
PEI	polyethylenimine
PET	Poly (ethylene terephthalate)
PSCs	Perovskite solar cells
Pt	Platinum
PTAA	poly (triaryl amine)
PV	Photovoltaic
QD	Quantum dot
QDs	Quantum dots
RF	Radio frequency
SnO2	Tin (IV) oxide or Tin dioxide
tBP	4-tert-butylpyridine
TEM	Transmission electron microscopy
TiO2	Titanium dioxide
TOL	Toluene
UV-VIS	Ultraviolet–visible spectroscopy
VB	Valence Band
XPS	X-ray photoelectron spectroscopy
XRD	X-ray diffraction
ZnO	Zinc oxide

LIST OF APPENDICES

Appendix A Characterization of spiro-OMeTAD

Appendix B Photovoltaic parameters of the fabricated solar cells (D5-D9**)**

FABRIKASI DAN PENCIRIAN SEL SURIA PEROVSKIT MEMPASIF DENGAN TITIK KUANTUM ZINK OKSIDA SEBAGAI LAPISAN PENGANGKUTAN ELEKTRON

ABSTRAK

Kajian ini didedikasikan untuk menghasilkan sel suria perovskit halida plumbum n-i-p bersuhu-rendah yang diproses menggunakan filem berasaskan titik kuantum (QD) ZnO sebagai lapisan pengangkutan elektron (ETL). Kajian ini dibahagikan kepada tiga bahagian utama seperti berikut: Bahagian pertama melaporkan pertumbuhan filem berasaskan QD ZnO bersuhu rendah dan filem perovskit halida plumbum ($CH_3NH_3PbI_3$) yang mana masing-masingnya sebagai lapisan ETL dan foto-aktif yang efisen. QD ZnO -ETL disediakan daripada QD ZnO berasaskan larutan yang mempunyai saiz zarah purata 4.4 nm menggunakan laluan solvoterma, kemudian disalut putar ke atas substrat ITO pada ketebalan yang berbeza dan dirawat pada suhu yang berbeza. Filem ZnO setebal 60 nm yang dikeringkan pada 100 ^oC menunjukkan kualiti yang lebih baik dari segi liputan permukaan, sifat semulajadi terpelihara QD dengan saiz butiran purata 5.13 nm, dan sifat fotoelektrik yang luar biasa disebabkan nisbah permukaan kepada isipadunya yang tinggi. Justeru ia dipilih sebagai ETL bersuhu rendah. Secara berasingan, filem perovskit $CH_3NH_3PbI_3$ ditumbuh pada suhu yang berbeza menggunakan pelarut dimetilformamida (DMF) dan dirawat dengan anti-pelarut yang berbeza. Analisis menunjukkan bahawa filem perovskit dirawat klorobenzena (CB) yang ditumbuh pada 100 ^oC mendedahkan morfologi permukaan bebas lompong dengan kehabluran dan sifat optik yang baik, oleh itu ia dipilih sebagai penyerap cahaya boleh lihat yang efisen dalam fabrikasi PSCs. Dalam bahagian kedua, filem $CH_3NH_3PbI_3$ yang dirawat CB

dan disempuhlindap pada 100 ^{o}C telah disepadukan pada QD ZnO -ETL setebal 60 nm untuk fabrikasi PSC tanpa lapisan dan dengan lapisan pasif Al_2O_3 (~10 nm) yang dimasukkan ke dalam antara muka QD ZnO-ETL/$CH_3NH_3PbI_3$. Keputusan menunjukkan bahawa pempasifan antara muka ZnO/perovskite menghalang kecacatan antara muka (kumpulan hidroksil dikurangkan daripada 30.7% kepada 11.04% ekoran pempasifan antara muka), yang membawa kepada kecekapan penukaran kuasa (PCE) yang dipertingkatkan daripada 2.76 kepada 6.02%. Bahagian ketiga membincangkan peningkatan selanjutnya dalam PCE dengan menambah baik kualiti morfologi permukaan lapisan perovskit yang tumbuh pada QD ZnO-ETL dengan menambahkan dimetil sulfoksida (DMSO) ke dalam pelarut DMF dalam nisbah isipadu yang dioptimumkan sebanyak 8%. Ini menghasilkan pertumbuhan lapisan perovskit yang padat dengan butiran yang lebih besar, meningkatkan PCE peranti bukan pasif kepada 11.32%. PCE telah dipertingkatkan lagi kepada 13.65% dan 17.28% dengan pempasifan bukan organik (Al_2O_3) dan organik (1wt.% polyethyleneimine, PEI) keatas antara muka ZnO/perovskite. Peningkatan yang luar biasa dalam PCE (22.09%) telah direkodkan apabila QD ZnO ETL ditumbuh di atas lapisan benih RF-ZnO (~15 nm) dan antara muka QD ZnO-ETL/Perovskite telah dipasifkan dengan lapisan PEI 1wt.%. Lapisan benih ZnO meningkatkan lagi kepadatan dan pertumbuhan bijian penyerap cahaya, membawa kepada pengurangan selanjutnya dalam perangkap pembawa cas dan laluan kebocoran semasa (pembentukan lubang jarum), dengan itu prestasi fotovolta yang lebih tinggi boleh diperolehi.

FABRICATION AND CHARACTERIZATION OF PASSIVATED PEROVSKITE SOLAR CELL WITH ZINC OXIDE QUANTUM DOTS AS ELECTRON TRANSPORT LAYER

ABSTRACT

This work is dedicated to fabricate low-temperature processed n-i-p lead halide perovskite solar cells using ZnO quantum dot (QD)-based film as electron transport layer (ETL). The work is divided into three main parts as follows: The first part reports the growth of low temperature ZnO QD-based film and lead halide perovskite ($CH_3NH_3PbI_3$) film as an efficient ETL and photo-active layer, respectively. The ZnO QD-ETL was prepared from solution-based ZnO QDs having average particle size of 4.4 nm using solvothermal route, then spin coated over ITO substrate at different thicknesses and treated at different temperatures. 60 nm-thick ZnO film dried at 100 ^oC showed better quality in terms of surface coverage, QD-preserved nature with average grain size of 5.13 nm, and outstanding photoelectric property due to its high surface-to-volume ratio, thus it was selected as low temperature ETL. Separately, $CH_3NH_3PbI_3$ perovskite films were grown at different temperatures using dimethylformamide (DMF) solvent and treated with different anti-solvents. The analysis showed that chlorobenzene (CB)-treated perovskite film grown at 100 ^oC revealed void-free surface morphology with good crystallinity and optical properties, thus it was chosen as an efficient visible light-absorber in the fabricated PSCs. In the second part, CB-treated $CH_3NH_3PbI_3$ film annealed at 100 ^oC was integrated over 60 nm-thick ZnO QD-ETL for fabricating PSCs without and with inserting Al_2O_3 passivating layer (~10 nm) into ZnO QD-ETL/ $CH_3NH_3PbI_3$ interface. The results

revealed that the ZnO/perovskite interface passivation suppresses the interfacial defects (hydroxyl group reduced from 30.7% to 11.04% upon interface passivation), leading to enhanced power conversion efficiency (PCE) from 2.76 to 6.02%. The third part discusses the further enhancement in the PCE by improving the surface morphology quality of the perovskite layer grow on ZnO QD-ETL by adding dimethyl sulfoxide (DMSO) into the DMF solvent in optimized volume ratio of 8%. This resulted in growth of densely packed perovskite layer with bigger grains, promoting the PCE of non-passivated device to 11.32%. The PCE was further enhanced to 13.65% and 17.28% upon inorganic (Al_2O_3) and organic (1wt.% polyethyleneimine, PEI) passivation of ZnO/perovskite interface. A remarkable enhancement in the PCE (22.09%) was recorded when ZnO QD-ETL was grown over RF-ZnO seed layer (~15 nm) and the ZnO QD-ETL/Perovskite interface was passivated with 1wt.% PEI layer. ZnO seed layer further enhances compactness and the grain growth of the photo-absorber, leading to further reduction in charge carrier traps and current leakage paths (pinhole formation), thus higher photovoltaic performance can be obtained.

CHAPTER 1

INTRODUCTION

1.1 Introduction

As industrial technology is growing fast worldwide, the consumption of fossil fuel energy is increasing heavily, which results in emission of high concentration of CO_2, leading to global warming and subsequent natural disasters. Therefore, the development of clean and eco-friendly energy sources is of high importance to sustain the life in our planet [1-3]. Among these clean eco-friendly energy sources, the solar energy is a promising and sustainable source to replace the non-clean fossil fuel energy [4, 5]. Solar cell technology is regarded as a direct and an effective method to convert solar energy into electricity through photovoltaic effect. Traditionally, crystalline silicon and thin film based solar cells have emerged as the sources of electrical energy from solar energy and referred as first and second-generation solar cells, respectively [6, 7]. However, due to their complication in the production process, high cost and low conversion efficiency, researchers started exploring new materials as third generation solar cells with high conversion efficiency and simple fabrication. These comprises dye sensitized solar cells, quantum dot solar cells, organic photovoltaics, and perovskite solar cells [8-10]. Among these, perovskite solar cells have emerged as a promising material for converting the solar energy into electrical power with high efficiency as compared to others [11-13].

1.2 Perovskite Solar Cells

Perovskite material, which is the photo-absorber in PSCs, is a type of crystalline architecture having the chemical formula of ABX_3 (A= CH_3NH_3, B=Pb or Sn and X=Cl, Br or I) as shown in Figure 1.1. Perovskite materials can be classified

as organic-inorganic lead halide perovskite [14], lead-free organic-inorganic halide perovskite [15], all inorganic lead halide perovskite [16], and lead-free all inorganic halide perovskite [17]. In this work, organic-inorganic lead halide perovskite ($CH_3NH_3PbI_3$) is used as photo-absorber owing to its bandgap corresponding to visible light and its excellent light absorption coefficient.

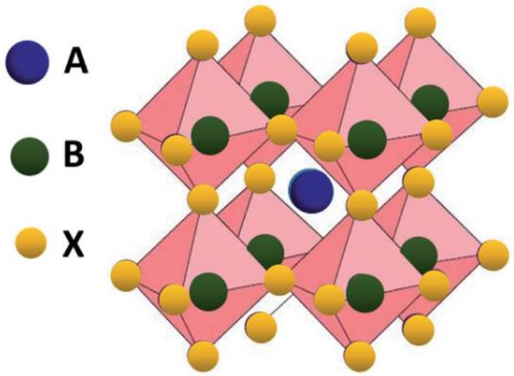

Figure 1.1 Crystal structure of organic-inorganic halide perovskite [18]

Solar cells based on perovskite material as a light absorbing layer have recently emerged as a promising candidate of semiconductor solar cells. Compared to conventional organic and inorganic semiconducting materials, organic-inorganic hybrid perovskite exhibits interesting optical and electrical properties including;

1) a large Bohr radius, high dielectric constant and a weak exciton binding energy which promotes a quick dissociation of the photoinduced exciton into electron-hole pair at room temperature [19-21].

2) a long carrier diffusion length and a longer lifetime [22-24].

3) high absorption coefficient and direct band gap of 1.5 eV which gives it an advantage to be used as good light absorber in UV-Vis light range [25,26]. Due to the

above-mentioned unique properties, organic-inorganic perovskite materials are highly recommended in the next generation of photovoltaic solar cells.

1.3 Problem Statement

Low cost, highly efficient and stable perovskite solar cell is appealing tremendous world attention as the next generation source of electrical power. The quality of the perovskite absorbing layer depends on the quality of the sublayer electron transport layer (ETL). Therefore, it is of high importance to grow ETL that meets high photovoltaic performance of PSCs. Low-temperature processed ZnO is an attractive candidate as ETL in low cost and flexible PSCs, owing to its high charge mobility, high transparency in visible light and good compatibility with perovskite layer in terms of band structure alignment and can be crystallized at relatively low synthesis temperature. However, low-temperature processed ZnO is still inferior as compared to TiO_2 and SnO_2 due to two main issues; first issue is the serious recombination at interface of ZnO/perovskite caused by the presence of high level of interfacial states and traps which can be significant for ZnO QD-based ETL due to the poor crystallinity, causing inhibition of charge transfer at interfaces. Second issue is the poor chemical stability at the interface between ZnO and perovskite material which is related to the presence of residual organic species on the surface of low-temperature processed ETL, leading to the deterioration of the PSCs photovoltaic performance. Different strategies, such as ZnO doping [27], mixing ZnO with additives to prepare nanocomposite ETL [28], coating ZnO surface with passivating layers [29], and preparing bi-layer ZnO-based ETL [30] have been adopted to tailor and engineer the ZnO/perovskite interface to better enhance the PSCs performance. However, the majority of the previous studies reported high temperature processed ZnO-ETL [31-

36], losing its valuable property in that it can be crystallize at low temperature using cost-effective preparation techniques which is beneficial for roll-to-roll low-cost PSCs fabrication. Preparation of efficient PSCs based on low-temperature processed ZnO QD-ETL remains a challenge and more research efforts are required.

1.4 Research Focus

The performance of PSCs can be controlled by many parameters such as, type of hole transport layer and electron transport layers (HTL, ETL), concentration and type of perovskite layer, and type of PSC architecture. Additionally, the HTL/Perovskite and ETL/perovskite interface quality plays a crucial role in the mechanism of photogenerated charge carrier transfer, stability, and the performance of PSCs. The research focus of this thesis is to prepare an efficient low-temperature processed ZnO QD-ETL and $MAPbI_3$ perovskite photo-absorber (Figure 1.2). Additionally, the ZnO/perovskite interface quality was rationally investigated and engineered to better enhance the power conversion efficiency of the PSCs. That engineered was done by using different passivation, non-organic material Aluminium oxide A_2lO_3 and organic material 1wt.% polyethyleneimine, PEI to improve the power conversion efficiency to 13.56% and 17.28% respectively.

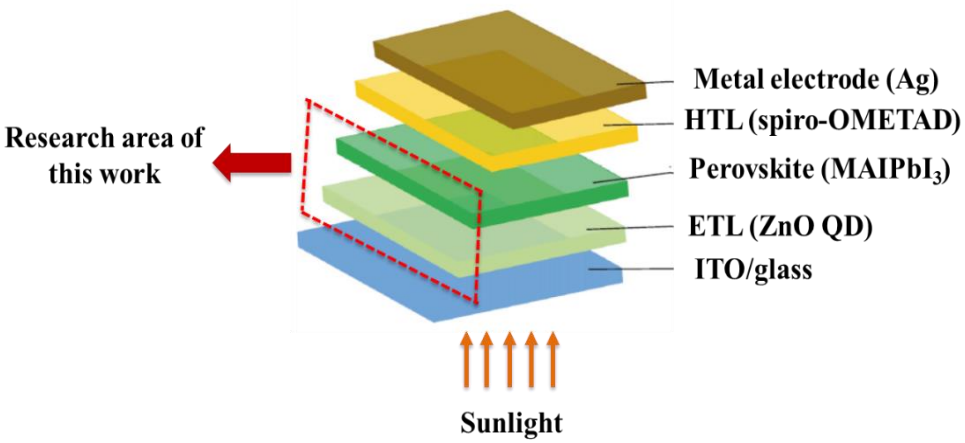

Figure 1.2 Schematic illustration of the research focus of this thesis

1.5 Research Objectives

The goal of this research work is to achieve three main objectives which are as follows:

1. To assess the optimized ZnO QD-based films as efficient ETL for PSCs through enhanced morphological, structural, optical, and photoelectric properties.

2. To estimate the optimized $MAPbI_3$ perovskite-based films as an efficient photo-absorber layer for PSCs through enhanced morphological, structural, and optical properties of the passivated and non-passivated perovskite.

3. To evaluate enhanced charge transportation and PCE resulting from ZnO QDs/$MAPbI_3$ interface passivation and different architectures in fabricated PSCs.

1.6 Originality of the Study

All low-temperature processed PSCs are of paramount importance in smart and roll-to-roll generation of solar cells. This work is mainly dedicated to fabricate all low-temperature PSCs using ZnO QD-based film as electron transport layer. The originality of this work is summarized in the following points:

1. Using sputter Al_2O_3 passivated low-temperature processed ZnO QD-ETL to fabricate an efficient PSC, which was not reported before and the obtain efficiency was 13.56%.
2. Utilizing polyethylenimine (1 wt% PEI) as a passivation layer at the interface of low-temperature processed ZnO QD-ETL/$MAPbI_3$, so that high efficiency (17.24%) was recorded.

3. Enhancing the surface morphology and the grain growth of perovskite photo-absorber through controlling DMSO solvent ratio to 8%,so that higher photovoltaic performance was obtained.
4. Growing low-temperature processed 1wt% PEI passivated ZnO QD-ETL over RF-sputtered ZnO seed layer to enhance the grain growth and reduce pinholes, resulting in further improvement in efficiency (22.2%).

1.7 Thesis Outline

This thesis comprises six chapters which are detailed as follows:

Chapter 1 provides an overview of perovskite based solar cells and their classification. The real problem faced in fabrication of efficient perovskite solar cells is also described in this chapter. In addition, the research focus and the objectives of this thesis are highlighted.

Chapter 2 gives a background on the history and type of solar cells. It also focuses on perovskite solar cells and their components and architectures. Additionally, it describes the working principle of perovskite solar cells and the photovoltaic characteristics used to evaluate their performance. A literature review on using ZnO material as ETL and the strategies used to enhance ZnO/perovskite interface quality are detailed in this chapter.

Chapter 3 introduces the methodology to prepare ZnO QD-based ETL, perovskite photo-absorber, and the perovskites solar cell fabrication procedure. The characterization instrumentation and the photovoltaic measurement setup are also included in this chapter.

Chapter 4 presents the results and discussions of ZnO QD-based films at different thicknesses and different growth temperatures. In addition, the photoelectric

characteristics of the prepared films are investigated in this chapter. The aim is to optimize the growth parameters of ZnO QD-ETL so that the photovoltaic performance of fabricated PSCs can be boosted.

Similarly to chapter 4, chapter 5 highlights the results and discussions of the $MAPbI_3$ perovskite photo-absorber grown at different temperatures and treated with different types of anti-solvents to optimize the photo-absorber quality. The $MAPbI_3$ perovskite layer is integrated over ZnO QD-ETL and PSCs with different configurations are fabricated and characterized; this comprises HTL-free and HTL included n–i–p PSCs. The enhancement in the $MAPbI_3$ perovskite quality and their photovoltaic characteristics are analyzed in this chapter. Furthermore, ZnO QD-ETL/ $MAPbI_3$ perovskite interface is carefully engineered through insertion of inorganic and organic passivation layers to promote the photogenerated e–h pairs transportation.

Chapter 6 concludes the results obtained in this thesis and introduces recommendations for future works.

CHAPTER 2

THEORETICAL BACKGROUND AND LITERATURE REVIEW

2.1 Introduction

This chapter provides analysis of PSCs, including their many varieties, theoretical foundations, and basic characteristics. The text explores the operating processes of PSCs and their component elements, offering a comprehensive explanation of how they work. Furthermore, the chapter discusses the difficulties faced by PSC technology. The various materials used as ETL and HTL and their importance specifically ZnO ETL, emphasize its crucial function and investigate various methods to improve its effectiveness in PSCs. A thorough literature study assesses how well PSCs function when combined with different ETL materials, offering useful insights into their use and improvement.

2.2 Solar Cell Generations

In recent years, solar cells have become a crucial factor in the worldwide transition to renewable energy. The progress made in materials and various manufacturing methods has greatly impacted the evaluation process. Nevertheless, there is still a multitude of obstacles that must be overcome before solar cells can effectively provide environmentally friendly and affordable electricity. The primary focus of research in this domain is on advancing solar cell technology, with particular emphasis on developing exceptionally efficient solar cells. These options include of multi-junction cells, printable solar cell materials like quantum dots, and graphene, which is a good material for an intermediate layer in solar cells because of its chemical stability and high conductivity. Graphene can serve as both an ETL and a HTL. Cost-

effective manufacturing and excellent light transmission [37-39]. Solar cells primarily function to absorb sunlight and convert it into electrical energy via the photovoltaic effect. The production process of solar cells encompasses several techniques that alter materials to enhance the solar cell performance. Various materials and strategies have resulted in the classification of solar technology into three separate generations [40], (Figure 2.1).

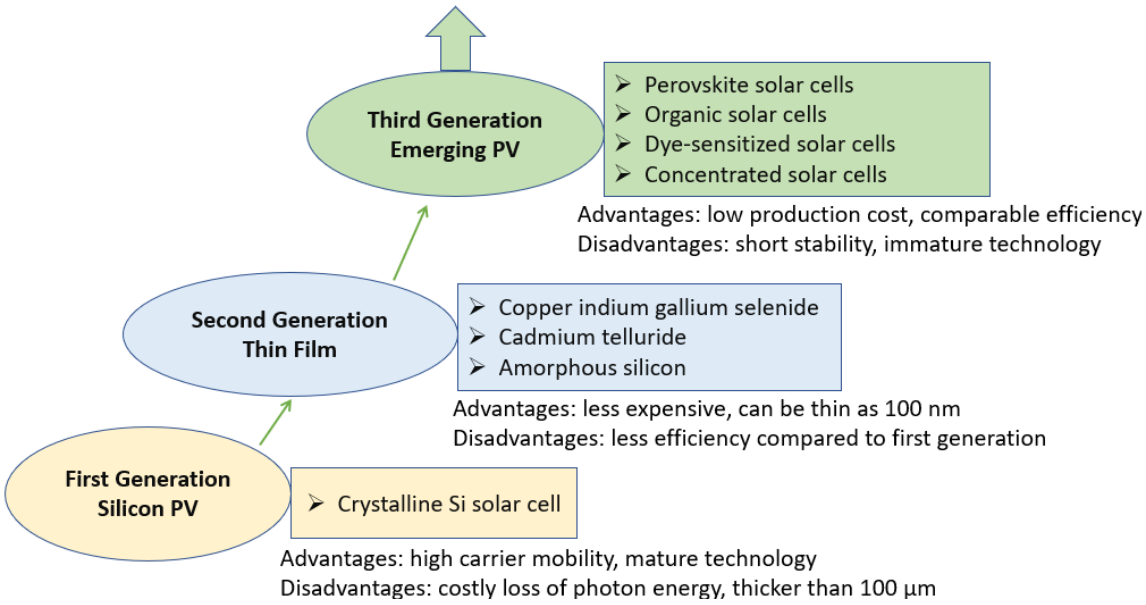

Figure 2.1 The three generations of solar cells

So far, solar cells classified into a variety of generations, the first class of solar cells was comprised of silicon (Si)-based PV cells. Currently, solar cells using silicon make up over 80% of the total installed capacity worldwide and dominate 90% of the market with efficiency (10-30%). Thus, it leads to the worldwide solar-cell industry because of its strong performance and reliability [41]. However, the first type of solar cell consists of thick crystalline layers consisting of Si. The current generation

primarily relies on mono-, poly-, and multi crystalline silicon, together with single III-V junctions (GaAs) [41, 42]. Furthermore, a second category of economically viable alternatives to traditional crystalline silicon cells has been developed, known as thin film photovoltaic cells. These cells utilise materials such as amorphous silicon, CdTe, copper indium gallium selenide (CIGS), and have a lower efficiency range of 13-23% [43]. These films have enhanced mechanical properties that make them ideal for various applications [41,43].

The third generation, which entails high-efficiency tandem, perovskite, dye-sensitized, organic, and developing ideas, embodies a diverse approach to solar cell technology. It also includes advanced technologies that go beyond the Shockley–Queisser limit of efficiency (31–41%). These range from tried-and-true ideas like multijunction or tandem structures to more theoretical ones like hot carrier, down-/up conversion, and multiple carrier generation effects. PSCs have recently attracted scientists' attention because they can work almost as well as high-performance silicon- and other artificial material-based solar cell technologies. This contrasts with organic and dye-sensitized solar cells. While, PSC devices have already reached 25% power transfer efficiency, which is a big step forward in just 10 years of research. Also, PSC technology is very appealing for meeting the world's future energy needs because of its cost-effectiveness [41,43,44].

2.3 Classification of Perovskite Solar Cells According to Their Architecture

PSCs can be categorized into many classes according to their structures, as illustrated in Figure 2.2. The two primary architectures used in PSCs are mesoporous

and planar, with further classifications based on the arrangement of the electron ETL and HTL to incident sunlight.

(i) Mesoporous Architecture: In mesoporous PSCs, the perovskite layer is typically deposited onto a mesoporous scaffold (such as TiO_2 or ZnO), which provides both structural support and an additional pathway for charge transport. The mesoporous structure allows for better infiltration of the perovskite material, which can enhance the overall light absorption and efficiency of the cell. The mesoporous scaffold also improves charge carrier collection, as it reduces recombination losses by facilitating the migration of electrons through the mesoporous network.

(ii) Planar Architecture: In planar PSCs, the layers are deposited onto a flat, continuous substrate without the use of a mesoporous scaffold. The perovskite layer is deposited directly onto a compact ETL. This design simplifies the fabrication process and can be more easily adapted for large-area production, but it may face challenges with charge carrier collection and interface quality compared to mesoporous structures.

Both architectures can be further categorized based on the orientation of the ETL and HTL relative to the incident sunlight, leading to two configurations:

- n-i-p Architecture: In this architecture, the ETL is oriented towards the incident light, while the HTL is placed on the opposite side of the perovskite layer. The "n" refers to the n-type material (ETL), the "i" represents the intrinsic perovskite layer, and the "p" refers to the p-type material (HTL). This architecture is commonly used in both mesoporous and planar PSCs and is known for offering improved electron extraction.

- p-i-n Architecture: In contrast, the HTL faces the incident light, with the ETL on the opposite side. The "p" refers to the p-type material (HTL), the "i" to the perovskite layer, and the "n" to the n-type material (ETL). This configuration is more commonly found in planar structures and is often used to optimize hole extraction and overall performance.

Furthermore, PSCs can also be classified into HTL-free or ETL-free architectures, depending on whether the corresponding layer is omitted. The study primarily focuses on HTL-free and n-i-p architectures, such as the ITO/ZnO QD/$CH_3NH_3PbI_3$/Ag configuration and the ITO/ZnO QD/$CH_3NH_3PbI_3$/Spiro-OMeTAD/Ag configuration.

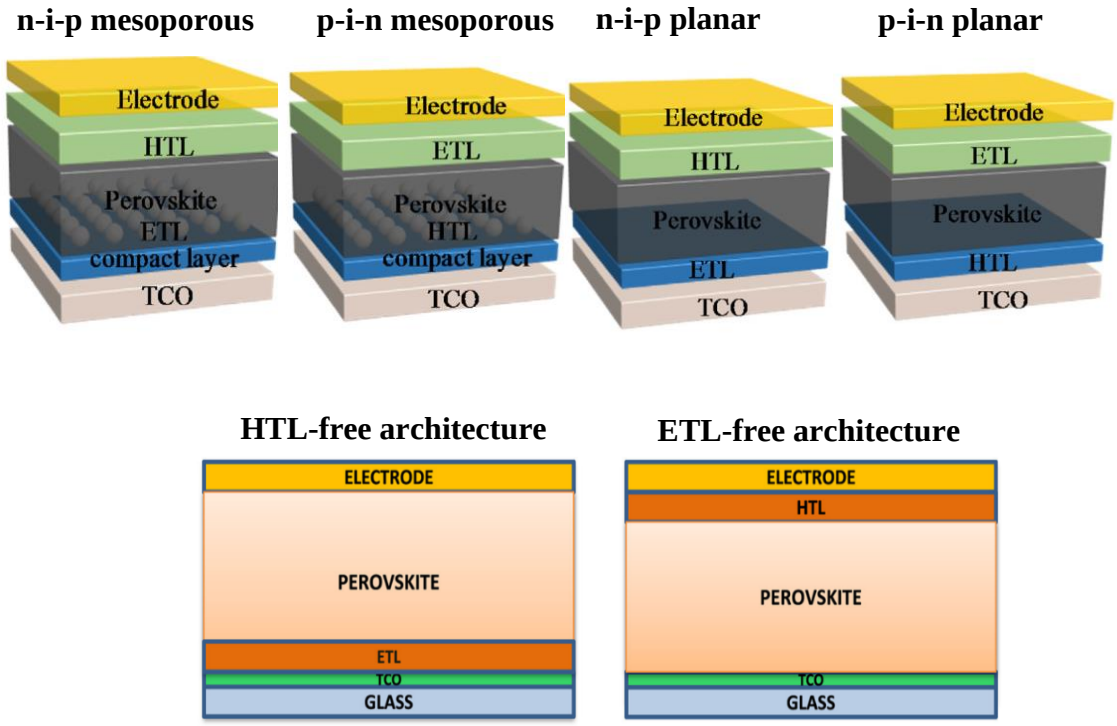

Figure 2.2 Different architectures of Perovskite solar cells with and without hole transport layer [45, 46] .

2.4 The Carrier Transport Materials

A PSC has an absorber layer in the middle of two very thin charge transport layers, called a HTL and an ETL. Additionally, electrodes are employed to gather electrons and holes. By analyzing the bands' energy level, electron affinity, and ionization potential, the band alignment can be determined. Hole transport materials are the ultra-thin layers with low electron affinities and ionization potentials, while ETLs are the ones with higher electron affinities and ionisation potentials. Therefore, a more thorough explanation of these layers is provided below [47,48].

2.4.1 The Hole Transport Layer

The HTL in PSCs has a crucial function in promoting the transfer of holes from the absorber layer and guiding them towards the electrode. In addition, the HTL functions as an electron-blocking layer, inhibiting the unwanted movement of electrons. A lot of different materials are used as HTLs. These include P3HT (Poly(3-hexylthiophene 2,5-diyl)), CuI (Copper(I) iodide), and CuSCN (Copper(I) thiocyanate) and Spiro-OMeTAD. The materials are chosen based on their ability to block electrons and their compatibility with the overall structure of the device, which helps to ensure the efficient functioning of PSCs [49-56].

2.4.2 Electron Transport Layer

The ETL in PSCs facilitates the transfer of injected electrons from the absober layer to the front electrode. Furthermore, the ETL functions as a protective layer, preventing the movement of holes towards the electrodes. The commonly employed electron transport layers comprise ZnO (Zinc Oxide), TiO2 (Titanium Dioxide), SnO2 (Tin (IV) Oxide), IGZO (Indium-Gallium-Zinc Oxide), and PCBM (6,6-phenyl-C61-butyric acid methyl ester). The materials are chosen based on their electron transport capabilities and their compatibility with the device structure, to guarantee effective charge transfer and collection in PSCs [49-52, 54, 55].

2.4.3 Electrodes

The cathode is an essential element in the structure of a solar cell that is responsible for gathering the carriers that are produced. The top electrodes as cathode commonly selected for their desirable properties in optoelectronic devices are ITO and FTO. These materials are favored because they have a low level of reflection, a high level of transmittance, excellent electrical conductivity, a high work function, and are easy to create patterns with. Acting as the electrodes, it enables the extraction of electrons when an electric current pass through the device. Similar to the cathode, the anode efficiently collects the generated holes from the absorption layer. When a current flow through the PSC, the cathode, whose transparency may vary depending on the kind of PSC, collects negative charged electrons. Al, Ag, Au, and Pt are examples of highly stable anodes with low work functions. These metals are frequently employed as anodes [56-59].

Thus, in order to create PSCs that have excellent performance and understand how PV works, it is crucial to understand the basic processes or stages that occur in the PSC layers and the function of each component [60]. The active layer absorbs some of the photons with energy higher than E_g that come into contact with the solar cells [61]. Perovskites exhibit variations in the binding energies of excitons, which allows for exciton interaction resulting in the formation of additional excitons or the generation of free holes and electrons to produce electric current [62]. Electron-hole pairs are created inside the field area and then separated due to the impact of this field. Consequently, the holes migrate towards the p-side while the electrons go towards the n-side. Electrons and holes accumulate along the borders of the p-n sides field areas, leading to their ultimate neutralization. The leftover charge carriers are sent to the load via the external circuit [63]. The HTL collects the unoccupied spaces for charge carriers, while the ETL collects the electrons. This is then followed by the electrodes.

2.5 Performance Properties and Main Parameters in PSCs

In PSCs, the main variables often used to assess the effectiveness of device that is mainly refer to the output characteristics such as V_{OC}, I_{SC}, FF, and PCE. These parameters collectively illustrate the device's behaviour and efficiency under various operating conditions. Thus, from the IV characteristic curve can obtain some physical parameters such as [64]:

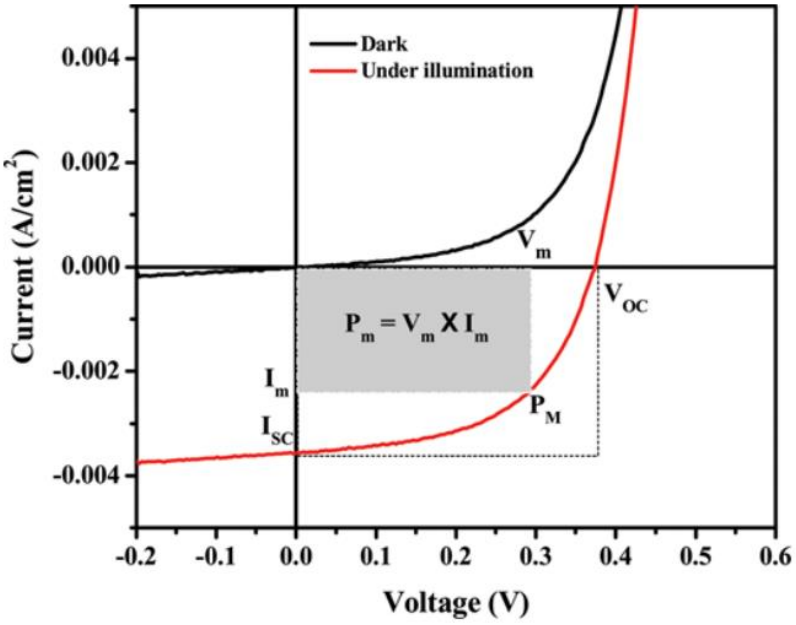

Figure 2.3 I-V characteristic response of perovskite solar cell showing the basic parameters of the solar device [65].

2.5.1 Open-Circuit Voltage

The V_{oc} refers to the highest achievable voltage output of solar cells. The applied bias nullifies the solar cell's inherent potential, hence eliminating the driving force for the collection of produced charges at V_{oc}. Consequently, there will be an absence of electric current (I=0) passing via the external circuit of the devices at Voc. It refers to the difference between the HOMO of the donor and the LUMO of the acceptor material [66].

2.5.2 The Short-Circuit Current

The J_{sc} represents the maximum current generated by a solar cell when exposed to a standard light source under zero-voltage conditions, where the cell’s terminals are

shorted. J_{sc} is a critical parameter as it indicates the ability of the cell to generate and transport charges (electrons and holes) efficiently. It reflects the total number of charge carriers produced in the active layer, separated, and successfully transported to the electrodes where they are collected as current solar cells, J_{sc} is influenced by factors such as light absorption, the mobility of charge carriers, and the quality of the donor-acceptor interface, where initial charge separation occurs. A high J_{sc} is typically desired, as it enhances the overall PCE of the device [67].

2.5.3 Fill Factor

While the J_{sc} and V_{oc} values correspond to the maximum current and voltage output of a solar device, it is important to note that no power is created at these locations. The FF is the metric that correlates these two quantities to ascertain the solar cell's maximum power output. It is a measure of the efficiency and determines the maximum power point (P_{max}) and V_{oc}. The FF of the solar cell can be determined by the values of the series resistance (R_s) and shunt resistance (R_{sh}) as well. It quantifies the extent to which the solar cell deviates from ideal behavior. Graphically, it represents the ratio of the size of the greatest rectangle which can constructed inside the J-V curve to the area of the rectangle generated by multiplying V_{oc} by J_{sc} as shown in Figure 2.3 [68].

$$FF = \frac{P_{max}}{V_{oc} \times I_{sc}} \tag{2.1}$$

The output power of the device, denoted as (P_{max}), is equal to the product of I_{max} (maximum current) and V_{max} (maximum voltage). The P_{max} is achieved when the current and voltage combinations provide the highest level of power. It does not happen when the V_{OC} or when it is I_{SC}. At the I_{SC} condition, the voltage across the cell

is ideally zero. Similarly, at the V_{OC} condition, the current flowing through the cell is also regarded to be ideally zero. Therefore, P_{max} does not occur at the maximum current. Instead, it occurs at a specific current that is lower than I_{SC} and lower than the V_{OC} [69].

2.5.4 The Power Conversion Efficiency

PCE is a key measure used to evaluate how effectively a solar cell converts sunlight into electrical energy. It is calculated by dividing the maximum power output (P_{max}) of the solar cell by the input power from sunlight (P_{in}), typically measured under standard conditions (AM1.5G, 1000 W/m²). The formula for PCE is (see equation 2.2) [70].

$$PCE = \frac{P_{out}}{P_{in}} \times 100\% \quad (2.2)$$

While, P_{max} depends on three main factors: J_{sc}, V_{oc}, and the FF:

$$P_{max} = J_{SC} \times V_{OC} \times FF \quad (2.3)$$

2.5.5 Series Resistance and Shunt Resistance

Throughout the cell, charge carriers pass across all the layers, which results in the phenomenon known as series resistance. Instead of having several resistances, they are all grouped into a single resistance, which simplifies the calculation process but makes it more difficult to identify which resistance is the source of the issues. To get the best performance from the cells, the R_s should be as low as feasible. This will allow the charge carriers to pass freely throughout the cell. The slope of the IV-curve at the V_{OC} is what defines the R_S, and the figure 2.3 shows how the IV-curve changes as the

R_S increases. It is important to ensure that the R_{sh} is as high as possible to prevent charge carriers from using alternate routes inside the cell. Due to charge carriers taking alternate pathways and recombining before they can be collected, the performance of the cell is significantly impacted when the R_{sh} is too low. This will cause the cell to work less effectively. A low R_{sh} is often the result of flaws in the cell, such as the presence of undesirable particles between layers or surface layers that decrease the device's performance [71].

2.6 Working Principle of PSCs

In recent years, many studies have investigated the dynamics of charge transport in PSC. These studies [72, 73], have also shown that excitons produced initially quickly separate into free charge carriers in picosecond. This excitation occurs due to the electric field which is produced because of the incident light absorption. Subsequently, the excitons are separated into delocalized charge carriers [74]. Moreover, the reason for the performance of the perovskite layer is the enhanced mobility of charge carriers inside the thin film medium, together with the efficient spread of electrons and holes across about 1 μm in the perovskite layer. This separation allows the charges produced by light to pass between the interface layer and electrode without being recombined [74]. Researchers have little knowledge of the generation and collection of charges in PSCs due to the intricate structure of the perovskite environment. The technique used to characterize silicon solar cells is also employed to explain the features of PSCs.

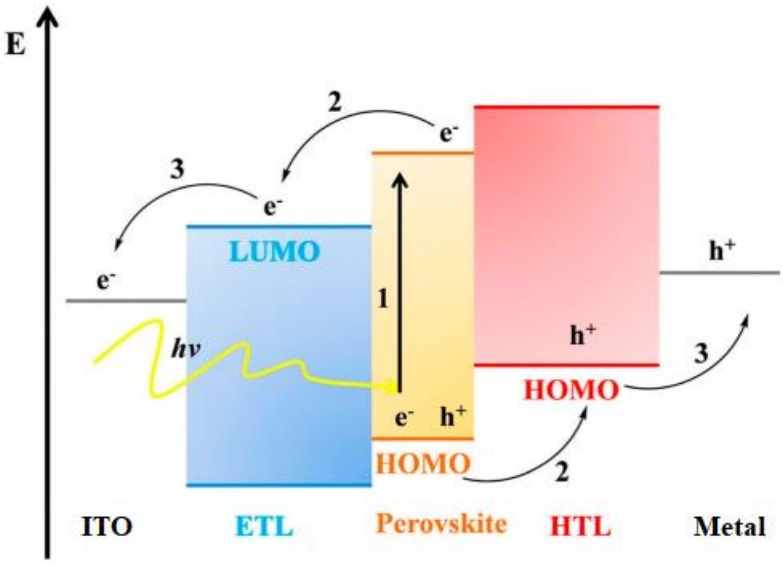

Figure 2.4 Energy band diagram of a typical n-i-p perovskite solar cell [72].

PSC devices typically undergo characterization through four main stages:

(a) The absorption of photons and the production of excitons.

(b) Diffusion and excruciating of excitons.

(c) The transfer of charges.

(d) The collecting of charges [75, 76]. Electron hole pairs are produced when photons hit the absorber layer.

Electrons and holes are created when excitons inside the perovskite material are separated because their binding energies are different. At the boundary between the HTL and ETL, exciton separation takes place. When electrons are taken out of holes and put into the ETL, they typically make their way to the cathode electrode.

The anode, usually a metal, receives the holes that have been guided into the HTL as depicted in Figure 2.4 [77]. The metal electrode serves as a means of gathering electrons and holes, while the transport conducting oxide is connected to an external circuit to produce an electric current. Thus, the PSCs is affected by variables like the bandgap, charge carrier mobility, and the absorber layer [78].

2.7 Properties of Perovskite as Photo-Absorber Layer

The PSC has emerged as one of the most remarkable cells in terms of efficiency. It has useful characteristics such as flexibility, lightweight, and semitransparency. Spin coating, ultrasonic spray coating, chemical vapour deposition, inkjet printing, the interdiffusion method, and other fabrication techniques are also viable options. The standard operating procedure calls for a 1:1 molar ratio of methylammonium iodide to lead iodide in most cases. Nevertheless, the deposition of the precursors is carried out using several procedures that effectively passivate the boundary flaws and result in an enlarged grain size. In the case of a blend of several substances, they are combined with the precursors specified by the weight ratio [79]. The characteristics of perovskite as the active layer in PSCs include:

(a) High absorption coefficient, materials used in the absorber layer have a noteworthy absorption coefficient, enabling them to effectively absorb sunlight and produce a substantial amount of electron-hole pairs.

(b) Tunable Bandgap, perovskite materials' which can be changed, allowing them to absorb a wide range of incident light, including both the visible and near-infrared ranges.

(c) Increasing light absorption is important for increasing the device efficiency.

(d) High charge carrier mobility, enabling efficient electron and hole transport inside the material that most of perovskite materials characterized by having high mobility.

(e) Maximizing the collection of charge carriers at the electrodes and reducing charge recombination is essential for enhancing device performance.

(f) Low-Temperature Processing, perovskite materials may be treated at low temperatures, which is helpful for making solar cells on flexible and inexpensive substrates. Besides, it can easily undergo solution processing, enabling the formation of uniform and expansive films by methods including spin-coating, and inkjet printing. This characteristic is advantageous for the efficient and economical production of PSCs [79,80].

2.8 Type and Role of the HTLs in PSCs

A perfect material for PSC HTLs would have excellent photochemical and thermal stability in air, high hole mobility by nature, and energy levels that are in good alignment with the perovskite layer. The material should be solution-processed to create the HTL, particularly for usage in traditional (n-i-p) PSCs. To achieve scalable manufacturing and widespread commercial use, it is important to consider the materials used as HTL is cheap and is easy to for preparation [81,82].

As already mentioned, HTL should demonstrate strong compatibility with other layers in the device stack to enhance charge transport efficiency and reduce interface recombination. The material should have good film-forming characteristics to allow consistent and uniform deposition across vast surfaces for making devices. The materials should be chemically inert to prevent unwanted reactions with the perovskite or other components of the device, ensuring long-term dependability and

consistent performance. Furthermore, the importance of environmentally friendly green synthesis and non-toxic materials is growing in the advancement of next-generation solar technology. Hence, a comprehensive approach that considers these different characteristics is crucial in the pursuit of the optimal material for absorber layer of PSCs [83]. Figure 2.5 displays energy level and extensively utilized materials in PSCs. The specific topic is as follows.

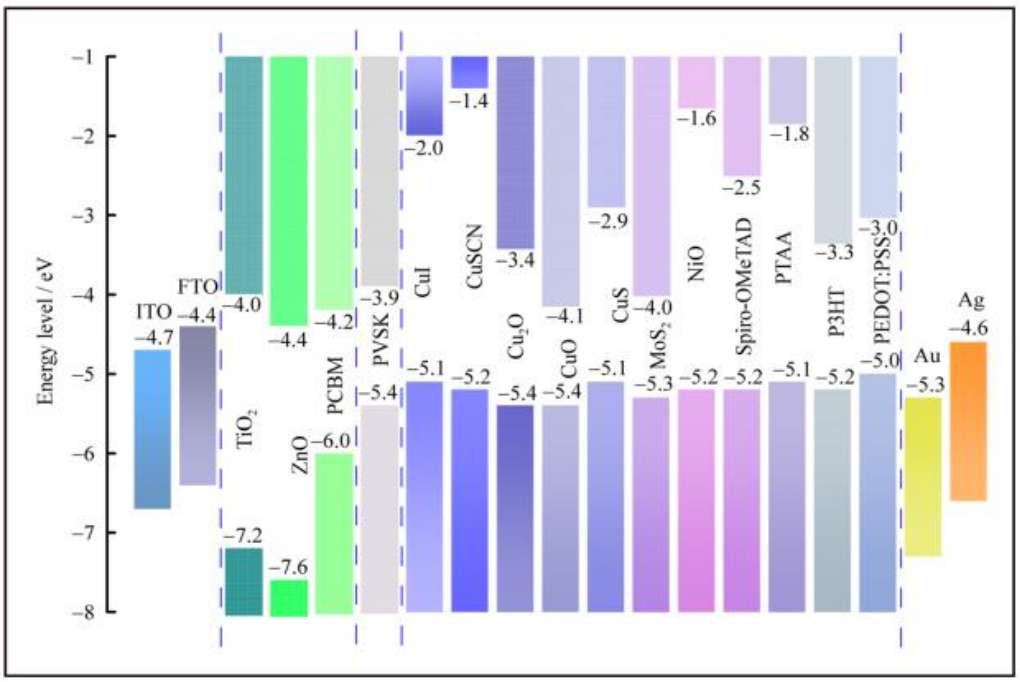

Figure 2.5 Energy level diagrams of HTL and ETL materials used in PSCs [84].

2.9 Type and Role of the ETL in PSCs

The ETL is crucial in enhancing the efficiency of photovoltaic systems. In order to reduce carrier recombination, it helps charges flow from the perovskite layer to the electrode while simultaneously blocking their migration to the counter electrode.

[85]. The primary criteria for choosing an ETL for PSC is to completely meet the following characteristics:

(i) The material used for ETL in PSCs is designed to prevent any chemical interaction with the cathode electrodes and light absorption in the perovskite layer.

(ii) The ETL material should ideally possess a compact morphology without any pinholes to prevent current leakage via these defects in the films.

(iii) The material used for ETL should have a lower empty molecular orbit level compared to the absorbing layer, which imparts a solid electron-accepting characteristic (Figure 2.4) [86].

2.10 Properties of ZnO as ETL in PSCs

ZnO is a semiconductor material that has proven highly suitable for photovoltaic applications, particularly as an electron transport layer (ETL) in perovskite solar cells (PSCs). It has a wide bandgap of 3.37 eV, which results in high electron mobility and favorable optoelectronic properties. Its conduction band energy level of 4.2 eV is well-suited to facilitate efficient electron extraction from the perovskite layer.

The wurtzite (hexagonal) crystal structure of ZnO further enhances its functionality as an ETL. In comparison to TiO_2, a commonly used ETL material in PSCs, ZnO offers distinct advantages. ZnO demonstrates much higher electron mobility, typically in the range of 10–100 $cm^2/V \cdot s$, compared to TiO_2's range of roughly 1–10 $cm^2/V \cdot s$. This higher mobility in ZnO helps reduce charge recombination losses, improving the overall efficiency of PSCs. Additionally, ZnO does not require high-temperature annealing during thin-film fabrication, making it compatible with flexible substrates and reducing energy costs in the production process. The choice to